


Generation of 30 kbar hydrostatic pressure in Bi₂Te₃ thin films by uniaxial deformation and its effect on the band structure

R. Shneck,^{1,*} S. Nемов,² V. P. Drachev,³ L. Chernyak ,⁴ and Z. Dashevsky¹

¹*Department of Materials Engineering, Ben-Gurion University of the Negev, Beer-Sheva 84105, Israel*

²*Peter the Great St. Petersburg Polytechnic University, St. Petersburg 195251, Russia*

³*Skolkovo Institute of Science and Technology, Center for Design, Manufacturing & Materials, Nobel Strasse, Building 1, Moscow 121205, Russia*

and Department of Physics, University of North Texas, Denton, Texas 76203, USA

⁴*Department of Physics, University of Central Florida, Orlando, Florida 32816, USA*



(Received 29 June 2021; revised 22 August 2021; accepted 26 August 2021; published 20 September 2021)

Generation of ultrahigh hydrostatic pressure by application of a strong one-axis deformation is demonstrated in epitaxial Bi₂Te₃ films on a mica substrate. This was followed by measurements of transport properties in *n*-type Bi₂Te₃ as a function of temperature (100–300 K) and pressure of up to 30 kbar. This pressure allowed studies of the restructuring of the conduction band. The nonmonotonic pressure dependence of the Hall coefficient and the increase of electrical conductivity $\sigma(P)$ can only be explained using two subband structures in the conduction band: subbands of light and heavy electrons with a mobility ratio of 10. The gap between the electron subbands increases with the hydrostatic pressure.

DOI: [10.1103/PhysRevB.104.115137](https://doi.org/10.1103/PhysRevB.104.115137)

I. INTRODUCTION

Tetradymite Bi₂Te₃ compound is a traditional thermoelectric (TE) material for direct energy conversion between heat and electricity [1–3]. For the applications of TE technologies in waste heat recovery and solid-state cooling, *p*- and *n*-type TE materials are needed [4–7]. Performance of TE materials is determined by the dimensionless figure of merit [8]:

$$ZT = \frac{S^2\sigma}{\kappa}T, \quad (1)$$

where S , σ , and κ denote the Seebeck coefficient; electrical and thermal conductivity, respectively; and T is the absolute temperature. Therefore, the high power factor $PF = S^2\sigma$ and a small thermal conductivity κ are desired for high ZT . Many studies have been performed to improve the PF by low dimensionalization [9], Fermi level tuning [10,11], band convergence [12–14], and highly mismatched isoelectric doping [15].

The Bi₂Te₃ semiconductor is interesting not only from the viewpoint of thermoelectric applications, but it is also considered as a new class of materials—topological insulators [16,17], while the properties of the Bi₂Te₃ topological insulator have been extensively studied [18].

One of the effective techniques for studies of semiconductor band structure is based on the influence of hydrostatic pressure on the transport properties (Hall effect, electrical conductivity, etc.) [19]. In the present work, a nearly hydrostatic stress is obtained by applying a uniaxial force to an epitaxial Bi₂Te₃ thin film on a mica substrate [20]. A

systematic study of the effect of nearly hydrostatic pressure on the transport properties of Bi₂Te₃ thin films with different electron concentrations has been performed.

II. BAND STRUCTURE OF Bi₂Te₃ SEMICONDUCTOR COMPOUND

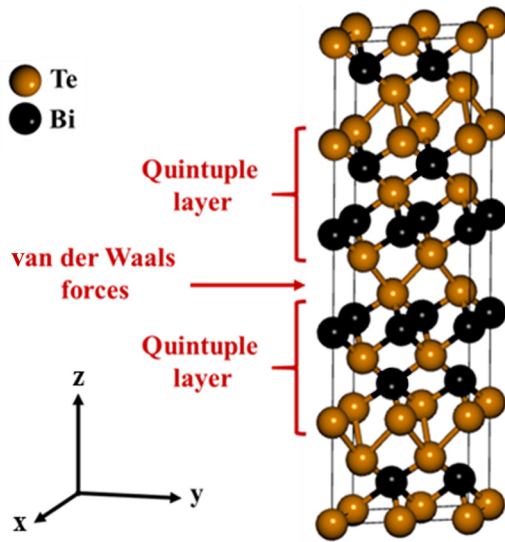
The crystal structure of Bi₂Te₃ consists of quintuple layers, which are perpendicular to the z axis in the hexagonal lattice, as shown in Fig. 1. Each quintet consists of five simple layers, where atoms interact one with another through covalent and ionic bonds. The quintuple layers are connected by weak van der Waals forces [15].

The band structure of the Bi₂Te₃ obtained using the density functional theory (DFT) approach was studied by several authors [e.g., 21–24]. The local density approximation (LDA) usually gives an underestimated band gap value of ~ 0.05 eV, which is quite far from the experimental value of ~ 0.13 eV. The LDA also shows an almost direct band gap located in the Γ - M direction of the Bi₂Te₃ Brillouin zone. Much better agreement with the experimental result of the band gap ($E_g = 0.12$ eV) has been obtained in [25] using the *GW* approximation. This approximation gives the conduction band minima in the Γ - Z direction, suggesting an indirect band gap. We discuss also the location of the first and second valence band maxima comparing with DFT calculations and angle-resolved photoemission (ARPES) measurements.

According to the optical data [26], Bi₂Te₃ is a non-direct-band semiconductor with a band gap $E_g \approx 0.13$ eV. The valence band is described by a two-band model with an energy gap $\Delta E_v \approx 0.02$ eV at $T = 300$ K [27].

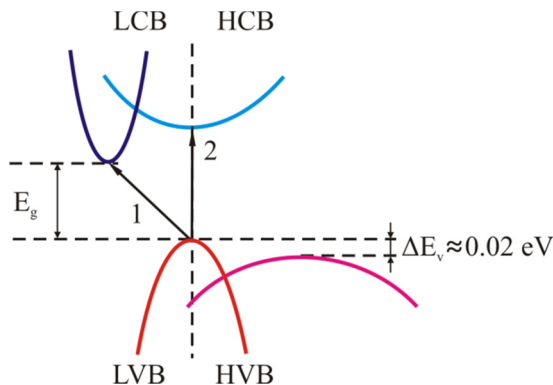
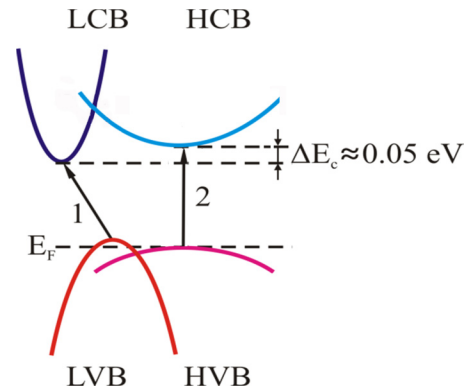
The reflection spectrum of *p*-type Bi₂Te₃ crystals doped with Sn is measured in [22]. The absorption spectrum

*roni@bgu.ac.il

FIG. 1. The crystal structure of Bi_2Te_3 .

calculated from the reflectance data using the Kramers-Kronig relations agrees with the experimentally obtained results. Analysis of the absorption spectra showed two types of optical transitions—indirect transitions with energy $E_1 \approx 0.14$ eV (close to the forbidden gap E_g) and direct transitions with energy $E_2 \approx 0.21$ eV. These data indicate a complex structure of the conduction band with an additional minimum located above the main minimum by the value of ΔE_c .

According to a recent work [28], the transport properties of the n -type $\text{Bi}_2\text{Te}_3/\text{Bi}_2\text{Se}_3$ can be explained only by using the two-band structure of the conduction band with different effective masses and weighted mobilities. Two options are possible for the interpretation of optical transitions in the Bi_2Te_3 band structure. The first option of the Bi_2Te_3 band structure is presented in Fig. 2. The light valence band (LVB) and the light conduction band (LCB) minima are in different \mathbf{k} points of the Brillouin zone (BZ). The heavy conduction band (HCB) and LVB minima are in one point of the BZ. The indirect transition 1 corresponds to the fundamental absorption in Bi_2Te_3 and determines its forbidden gap (the band gap) $E_g \approx E_1 \approx 0.14$ eV. The direct transition 2 with the energy E_2

FIG. 2. Schematic view of the band structure and optical transitions in Bi_2Te_3 according to option 1.FIG. 3. Schematic view of the band structure and optical transitions in Bi_2Te_3 according to option 2.

occurs from the main LVB to the additional HCB. Considering the aforementioned information, the edge between the two conduction bands (HCB and LCB) equals $\Delta E_c \approx 0.07$ eV.

The second option of the Bi_2Te_3 band structure is presented in Fig. 3. This option looks more truthful. The light valence band (LVB) and the light conduction band (LCB) minima are in different \mathbf{k} points of the Brillouin zone (BZ). The heavy conduction band (HCB) and LVB minima are in one point of the BZ. At room temperature, Fermi level E_F is located between the two valence bands (HVB and LVB).

The direct transition 2 with the energy E_2 occurs from the HVB to the HCB and is shown in Fig. 3. The edge between the two conduction bands (HCB and LCB) equals

$$\Delta E_c = E_2 - E_1 - \Delta E_v \approx 0.05 \text{ eV}, \quad (2)$$

where $\Delta E_v \approx k_b T \approx 0.026$ eV (k_b is the Boltzmann constant; T is the absolute temperature).

The pressure dependence of the transport properties over the temperature range of 100–300 K and under the hydrostatic pressure of up to 30 kbar presented in this work can provide a complete explanation of the structure of the conduction band in Bi_2Te_3 . Success in this task is important for the optimization of the transport properties of the classical thermoelectric Bi_2Te_3 based compounds.

III. EXPERIMENTAL PROCEDURE

Synthesis of Bi_2Te_3 was carried out by direct melting of high-purity elements for 10 h at 1073 K in sealed quartz ampoules evacuated to a residual pressure of 10^{-5} mbar. Each ampoule was then taken from the furnace and quenched in cold water. The obtained ingots were crushed into fine powders by ball milling in argon atmosphere. Bi_2Te_3 films with higher electron concentration were obtained in nonstoichiometric $\text{Bi}_{2-x}\text{Te}_{3+x}$ due to the donor effect of substitutional Te atoms replacing Bi atoms [29].

The n -type Bi_2Te_3 thin films were deposited using flash evaporation technology as described in [30,31]. The substrate temperature for film evaporation was $T_s = 523$ K; the evaporation velocity was $v_e = 0.1$ $\mu\text{m}/\text{min}$. After the evaporation process, all films were annealed in the same evaporation

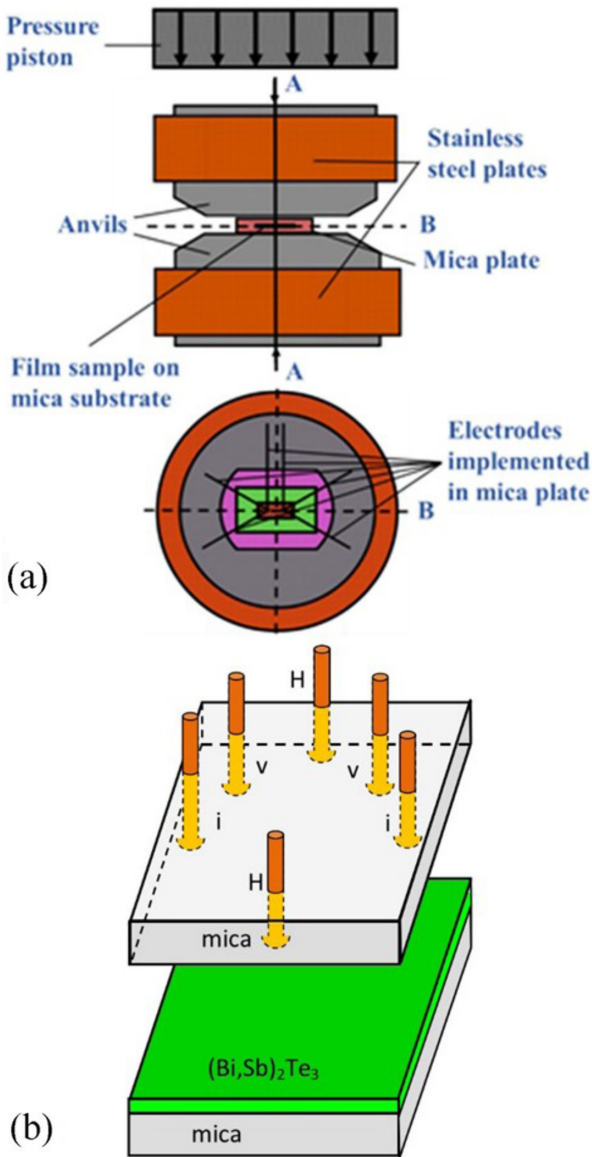


FIG. 4. (a) Schematic view of the device for measuring the transport properties of films under uniaxial deformation. (b) Schematic view of a sandwich of film specimen on a mica substrate and mica plate with copper contacts (contacts to measure: v —voltage drop, i —current, and H —Hall contacts).

chamber at $T_i = 623$ K for 0.5 h in a pure argon atmosphere under the pressure $p = 0.9$ atm.

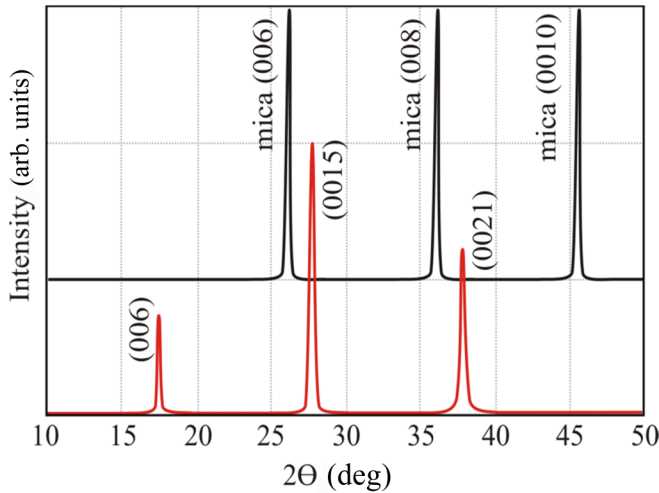
The structural analysis of the films was carried out by an x-ray diffractometer STOE STADI P (by STOE & Cie GmbH, Germany) with a modified Guinier geometry scheme using the transmission mode [$\text{Cu } K\alpha_1$ radiation, concave Ge monochromator (111) of the Johann type; $2\theta/\omega$ scan, angles interval with angle step of 0.015° and step time of 2 s]. The initial processing of experimental diffraction arrays was performed using POWDERCELL (rev. 2.4) software. Secondary emission electron images were taken with a Quanta 200 environmental scanning electron microscope (HRSEM).

For the investigation of the transport properties (Seebeck coefficient, S ; electrical conductivity, σ ; and Hall coefficient, R_H) of thin films at temperatures ranging from 80 to 500 K, a unique measurement setup was used [32]. The measurement of the Hall effect was carried out in permanent magnetic fields up to 2 T. The results were averaged using two opposite directions of the electrical and magnetic fields. The temperature accuracy was 0.1–0.2 K, and that of the magnetic field is 3%. The uncertainty of the Seebeck coefficient and electrical conductivity was 6%. The Hall effect was measured with an accuracy of 8%.

The creation of hydrostatic pressure due to a strong one-axis deformation of a semiconductor film on the thin substrate was originally proposed in [30] and developed in [33]. The schematic view of the measurement setup and the work principle are presented in Fig. 4. The setup is a type of Bridgman anvil with a few upgrades. The dimensions of the insulation substrate and the film were chosen so that the thicknesses of both were much smaller than their length and width. In this case, the deformation along the film can be neglected. The sample and the electrode system were located between layers of insulating material (mica). The typical sample size was $5 \times 3 \times 0.001$ mm; the dimensions of the insulating material were $15 \times 10 \times 0.1$ mm. The electrodes were made of flattened copper wire with a diameter of 0.02 mm, which is incorporated into the material. A solenoid was installed coaxially with the anvils, creating a magnetic field parallel to axis A. The magnetic core is the supporting structure of the press. Copper-constantan thermocouples are used to measure the temperature of the sample.

TABLE I. Relevant material properties of Bi_2Te_3 material and mica substrate.

Material	Crystal structure	Lattice parameters at $T = 300$ K	Thermal expansion coefficient at $T = 300$ K ($\times 10^6, \text{K}^{-1}$)	Elastic constants at $T = 300$ K, GPa	Reference
Bi_2Te_3	Hexagonal	$a = 0.519$ nm	$k = 12.9 \times 10^6$	$(C_{11} = 73.8, (C_{33} = 54.3,$ $C_{44} = 30.4, (C_{66} = 28.7,$ $C_{13} = 30.6, (C_{12} = 16.3$	[15]
Mica	Monoclinic	$a = 0.438$ nm $c = 3.049$ nm	$k = 7.5 \times 10^6$	$(C_{11} = 181, (C_{22} = 178,$ $C_{33} = 58, (C_{44} = 16,$ $C_{55} = 19.5, (C_{66} = 72,$ $C_{23} = 21, (C_{13} = 25,$ $C_{12} = 48, C_{15} = -14,$ $C_{25} = 1, C_{35} = 1,$ $C_{46} = -5.2$	[34]

FIG. 5. XRD spectra of Bi_2Te_3 film on mica substrate.

IV. RESULTS AND DISCUSSION

A. Structural properties

Mica (muscovite) has a monoclinic crystal structure (Table I) with a weak deviation from a cubic structure.

Figure 5 illustrates the x-ray diffraction patterns of the $1\ \mu\text{m}$ thick film of Bi_2Te_3 grown at $T_s = 523\ \text{K}$ and after annealing at $T_t = 623\ \text{K}$ during 0.5 h in argon atmosphere. The hexagonal Bi_2Te_3 film demonstrates a high-quality structure with preferred texturization in the (0001) direction (c axis parallel to the normal to the film plane), indicating an epitaxial growth of the Bi_2Te_3 film on the mica substrate.

B. Transport properties

Figure 6(a)–6(c) show the transport properties of $1 \pm 0.1\ \mu\text{m}$ thick $n\text{-Bi}_{2-x}\text{Te}_{3+x}$ films with different compositions corresponding to electron concentration n ranging from $4 \times 10^{18}\ \text{cm}^{-3}$ to $8 \times 10^{19}\ \text{cm}^{-3}$.

For obtaining the majority electronic carrier concentrations in the investigated films, Hall effect measurements were carried out in the temperature range of 100–300 K. Figure 6(a) shows the measurement results. The films show negative values of the Hall coefficient in the entire temperature range, confirming n -type electron conductivity in $\text{Bi}_{2-x}\text{Te}_{3+x}$ films. For all specimens, the absolute value of the Hall coefficient $|R_H|$ decreases with increasing temperature. For low electron concentration ($n = 4 \times 10^{18}\ \text{cm}^{-3}$), $|R_H|$ decreases by a factor of 2.

Figure 6(b) shows the Seebeck coefficient S for $n\text{-Bi}_{2-x}\text{Te}_{3+x}$ films as a function of temperature. The Seebeck coefficient has negative values over the investigated temperature range, which is typical for semiconductors with n -type conductivity. For samples 1 and 2, with lower electron concentrations, the maximum Seebeck coefficient close to $T = 300\ \text{K}$ is observed, which then starts decreasing due to the effect of minority carriers [15].

The electrical conductivity σ for $n\text{-Bi}_{2-x}\text{Te}_{3+x}$ films decreases with increasing temperature as shown in Fig. 6(c), indicating metallic behavior. The value of σ increases for higher electron concentrations over the investigated temperature range.

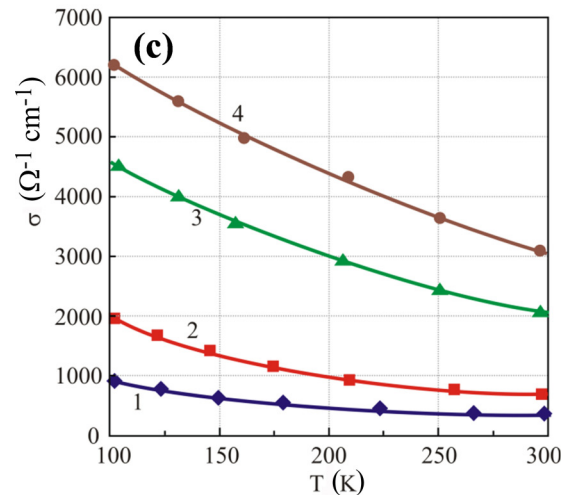
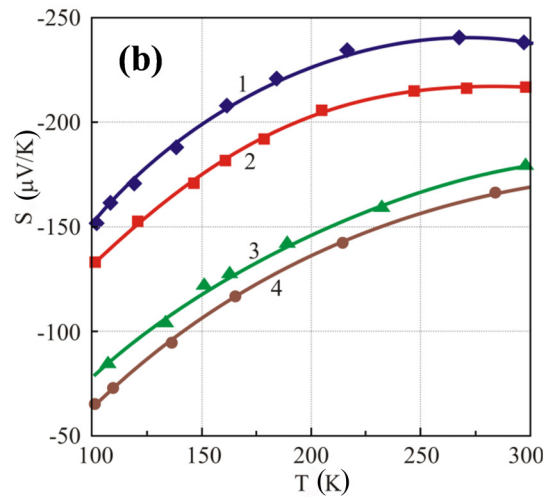
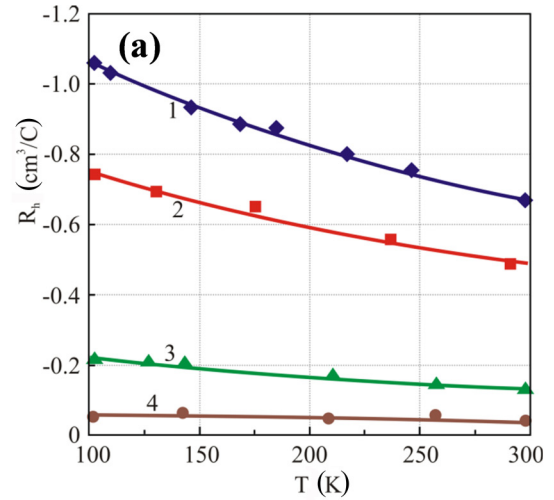


FIG. 6. Hall coefficient R_H (a), Seebeck coefficient S (b), and electrical conductivity σ (c) as a function of temperature for $n\text{-Bi}_{2-x}\text{Te}_{3+x}$ films on mica substrate. 1– $n = 4 \times 10^{18}\ \text{cm}^{-3}$; 2– $n = 7 \times 10^{18}\ \text{cm}^{-3}$; 3– $n = 3 \times 10^{19}\ \text{cm}^{-3}$; 4– $n = 8 \times 10^{19}\ \text{cm}^{-3}$.

C. Transport properties under strong compression

The study of semiconductor transport properties under strong compression is of considerable scientific interest. Typical high-pressure liquid chambers for measuring

transport properties of bulk samples can produce pressure below $P = 15$ kbar [19]. It is, therefore, very important to develop alternative research methods and measurement setups for producing higher pressure without sample destruction.

In a thin epitaxial film, two-dimensional epitaxial elastic stress prevails:

$$\hat{\sigma}_{epi} = \begin{pmatrix} \sigma_1 & & \\ & \sigma_2 & \\ & & 0 \end{pmatrix}. \quad (3)$$

Applying a normal compressive stress P induces Poisson expansion in the transverse directions in the film plane. When the uniaxial stress is applied to a small region of the film, the surrounding film and substrate constrain the Poisson expansion in the film (transverse) plane, thus causing compressive elastic stresses also in the film plane. These stresses, in the case of the isotropic material, can be roughly estimated from Hooke's law:

$$\varepsilon_{xx} = \frac{1}{E}[\sigma_{xx} - \nu(\sigma_{yy} + P)] = 0, \quad (4)$$

which yields, for $\sigma_{xx} = \sigma_{yy}$,

$$\sigma_{xx} = \frac{\nu}{1-\nu}P = 0.43P, \quad (5)$$

where E is the Young's modulus of the film. This indicates that the added stresses in the plane are approximately half the uniaxial pressure P . If the epitaxial stresses are compressive, the film may be closer to a hydrostatic state of stress.

$$\hat{\sigma}_{tot} = \begin{pmatrix} \sigma_1 + \frac{\nu P}{1-\nu} & & \\ & \sigma_2 + \frac{\nu P}{1-\nu} & \\ & & P \end{pmatrix}. \quad (6)$$

In this work, we applied pressure in the 0–30 kbar range which causes high elastic strains (up to $\varepsilon_{zz} \sim 6\%$) in $\text{Bi}_{2-x}\text{Te}_{3+x}$ films without sample destruction. This deformation is remarkably higher as compared to bulk samples where only $\sim 0.01\%$ strain can be obtained before breaking the material.

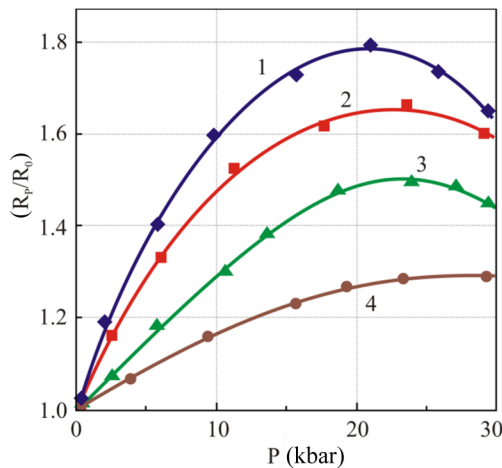


Figure 7(a) demonstrates the Hall coefficient and the electrical conductivity of n -type $\text{Bi}_{2-x}\text{Te}_{3+x}$ films on a mica substrate with different electron concentration as a function of pressure P at $T = 300$ K. The absolute value of the Hall coefficient $|R_H|$, for the films with electron concentration up to $n = 3 \times 10^{19} \text{ cm}^{-3}$, first increases until reaching a maximum and after that $|R_H|$ decreases with increasing pressure. For samples with higher electron concentration, the absolute value of the Hall coefficient decreases with increasing pressure in the entire pressure range. Figure 7(b) shows that the electrical conductivity increases with pressure increasing from 0 to 30 kbar for all compositions. The electrical conductivity for the sample with maximum electron concentration ($n = 8 \times 10^{19} \text{ cm}^{-3}$) shows a lower increase with pressure in comparison with the samples with lower electron concentration.

Figures 8(a) and 8(b) present the Hall coefficient and the electrical conductivity as a function of pressure for the n - Bi_2Te_3 film ($n = 4 \times 10^{18} \text{ cm}^{-3}$) at different temperatures in the 100–300 K range. For $T = 180$ K the pressure behavior of the Hall coefficient is the same as at $T = 300$ K. At $T = 100$ K, $|R_H|$ decreases with increasing pressure over all the pressure range. The electrical conductivity at $T = 100$ K shows a lower increase with pressure in comparison with the electrical conductivity at $T = 300$ K.

The transport properties are naturally interpreted within the framework of the two-band model of the conduction band in Bi_2Te_3 . The Hall coefficient R_H and σ can be represented as follows [23]:

$$R_H = R_{He}^h [\sigma_e^h / (\sigma_e^h + \sigma_e^l)]^2 + R_{He}^l [\sigma_e^l / (\sigma_e^h + \sigma_e^l)]^2, \quad (7)$$

$$\sigma = \sigma_e^h + \sigma_e^l, \quad (8)$$

where R_{He}^h and σ_e^h are the Hall coefficient and conductivity for heavy electrons. R_{He}^l and σ_e^l are the Hall coefficient and conductivity for light electrons.

The compression of the film increases the gap between the light and heavy electron subbands ΔE_g , as illustrated in Fig. 9, accompanied by the transition of electrons from the heavy to

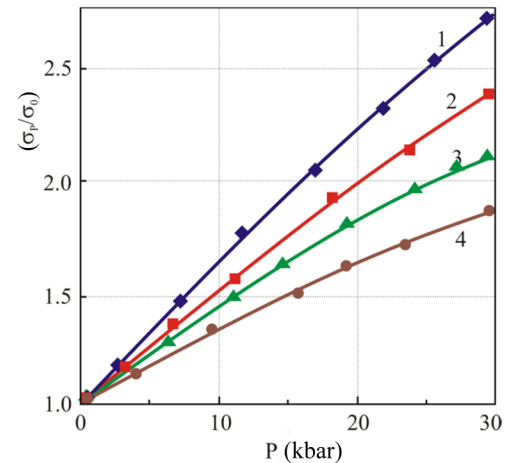


FIG. 7. The Hall coefficient R_H (a) and electrical conductivity σ (b) as a function of pressure for n - $\text{Bi}_{2-x}\text{Te}_{3+x}$ films on a mica substrate at $T = 300$ K. 1- $n = 4 \times 10^{18} \text{ cm}^{-3}$; 2- $n = 7 \times 10^{18} \text{ cm}^{-3}$; 3- $n = 3 \times 10^{19} \text{ cm}^{-3}$; 4- $n = 8 \times 10^{19} \text{ cm}^{-3}$.

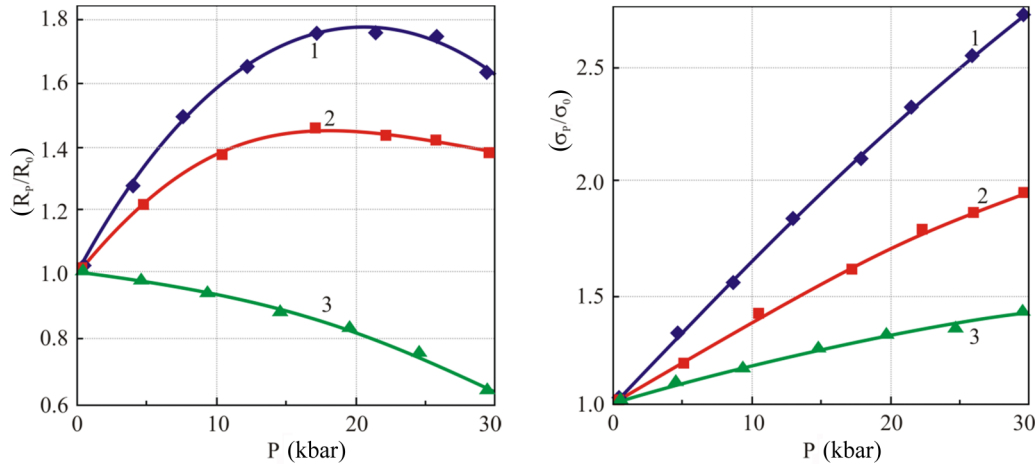


FIG. 8. The Hall coefficient R_H (a) and electrical conductivity σ (b) as a function of pressure for n - Bi_2Te_3 film ($n = 4 \times 10^{18} \text{ cm}^{-3}$) on a mica substrate over 100–300 K temperature range. 1– $T = 300$ K; 2– $T = 180$ K; 3– $T = 100$ K.

the light band. In the original state $\sigma_e^h > \sigma_e^l$ [Eqs. (7) and (8)]. An increase in the contribution of light electrons leads to an increase of the absolute value of the Hall coefficient $|R_{He}|$, the maximum of which is reached at $\sigma_e^h = \sigma_e^l$. $|R_{He}|$ then decreases with a further increase σ_e^l so that $\sigma_e^h < \sigma_e^l$ with growing pressure.

If the change of the total Hall coefficient $R(P)$ and the electrical conductivity $\sigma(P)$ are caused only by the redistribution between the light conduction band (LCB) and the heavy conduction band (HCB) (Figs. 2 and 9), it should be a clear relationship between relative growth of $|R|(P)$ and $\sigma(P)$ [23]:

$$\frac{R_{P^*}}{R_0} = \frac{(b+1)^2(b+A)^2}{4b(1+A)(b^2+A)}, \quad (9)$$

$$\frac{\sigma_{P^*}}{\sigma_0} = \frac{2b(A+1)}{(b+1)(b+4)}, \quad (10)$$

where the parameter A is the ratio between the electron concentration in HCB and LCB; $A = n_{h0}/n_{l0}$ and b is the ratio

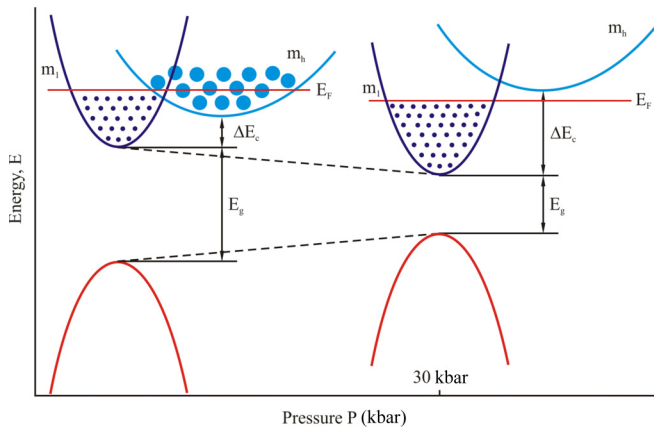


FIG. 9. Schematic view of the band structure restructuration as a function of the hydrostatic pressure in Bi_2Te_3 films on a mica substrate.

of Hall mobility of light electrons to the Hall mobility of heavy electrons; $b = \mu_l/\mu_h$ [23]. Index “0” corresponds to the pressure $P = 0$. At pressure P^* the electrical conductivity at the LCB equals the electrical conductivity in the HCB: $\sigma_l = \sigma_h$. From Eqs. (9) and (10) the following is obtained:

$$\frac{R_0}{R_{P^*}} = 2 \frac{\sigma_{P^*}}{\sigma_0} - \left(\frac{\sigma_{P^*}}{\sigma_0} \right)^2. \quad (11)$$

Following Eq. (11), the experimental value $R_{P^*}/R_0 \approx 1.8$, for the electron concentration $n = 4 \times 10^{18} \text{ cm}^{-3}$ (Fig. 7), corresponds to $\sigma_{P^*}/\sigma_0 \approx 2.2$, which is close to the experimental value $\sigma_{P^*}/\sigma_0 \approx 2.0$.

V. CONCLUSIONS

(1) A technique is presented for creation of a nearly hydrostatic pressure by a strong uniaxial deformation in epitaxial films on a mica substrate.

(2) A systematic study of transport properties (Hall coefficient, Seebeck coefficient, electrical conductivity) in n -type Bi_2Te_3 films with variable electron concentration has been carried out over the temperature range of 100–300 K and under the hydrostatic pressure of up to 30 kbar.

(3) The results are interpreted within the framework of the two-band model of the conduction band in Bi_2Te_3 , which demonstrates the increasing of the gap between the subbands of the light and heavy electrons due to the hydrostatic pressure.

ACKNOWLEDGMENT

The authors would like to thank Dr. Taras Parashchuk from AGH University of Science and Technology (Poland) for help with all parts of the investigation, and for useful advice and discussion.

- [1] J. Herremans and B. Wiendlocha, Tetradymites: Bi₂Te₃ and related materials, in *Materials Aspect of Thermoelectricity*, edited by C. Uher (CRC Press, Boca Raton, FL, 2016).
- [2] O. Ben-Yehuda, R. Shuker, Y. Gelbstein, Z. Dashevsky, and M. P. Dariel, High textured Bi₂Te₃-based materials for thermoelectric energy conversion, *Appl. Phys.* **101**, 113707 (2007).
- [3] O. Meroz, N. Elkabets, and Y. Gelbstein, Enhanced thermoelectric properties of *n*-type Bi₂Te_{3-x}Se_x alloys following melt-spinning, *ACS Appl. Energy Mater.* **3**, 2090 (2020).
- [4] I. T. Witting, T. C. Chasapis, F. Ricci, M. Peters, N. A. Heinz, G. Hautier, and G. J. Snyder, The thermoelectric properties of bismuth telluride, *Adv. Electron. Mater.* **5**, 1800904 (2019).
- [5] Z. Dashevsky and S. Skipidarov, Investigating the performance of bismuth-antimony telluride, in *Novel Materials and Device Design Concepts. Thermoelectric Power Generation*, edited by S. Skipidarov and M. Nikitin (Springer, New York, 2020), pp. 3–22.
- [6] T. Parashchuk, N. Sidorenko, L. Ivantsov, A. Sorokin, M. Maksymuk, B. Dzundza, and Z. Dashevsky, Development of solid-state multi-stage thermoelectric cooler, *J. Power Sources* **496**, 229821 (2021).
- [7] M. Maksymuk, T. Parashchuk, B. Dzundza, L. Nykyruy, L. Chernyak, and Z. Dashevsky, Highly efficient bismuth telluride-based thermoelectric microconverters, *Mater. Today Energy* **21**, 100753 (2021).
- [8] T. Parashchuk, I. Horichok, A. Kosonowski, O. Cherniushok, P. Wyzga, G. Cempura, A. Kruk, and K. T. Wojciechowski, Insight into the transport properties and enhanced thermoelectric performance of *n*-type Pb_{1-x}Sb_xTe, *J. Alloys Compd.* **860**, 158355 (2021).
- [9] Q. Zhang, G. Wu, Z. Guo, P. Sun, R. Wang, L. Chen, X. Wang, X. Tan, H. Hu, B. Yu, J. G. Noudem, G. Liu, and J. Jiang, Enhanced thermoelectric and mechanical performances in sintered Bi_{0.48}Sb_{1.52}Te₃-AgSbSe₂ composite, *ACS Appl. Mater. Interfaces* **13**, 24937 (2021).
- [10] Z. Ren, A. A. Taskin, S. Sasaki, K. Segawa, and Y. Ando, Fermi level tuning and a large activation gap achieved in the topological insulator Bi₂Te₂Se by Sn doping, *Phys. Rev. B* **85**, 155301 (2012).
- [11] K. T. Wojciechowski, T. Parashchuk, B. Wiendlocha, O. Cherniushok, and Z. Dashevsky, Advanced electronic structure engineering achieved by In and I doping in PbTe for the manufacture of a high-performance *n*-type thermoelectric leg, *J. Mater. Chem. C* **8**, 13270 (2020).
- [12] R. A. Masut, C. Andre, D. Vasilevskiy, and S. Turenne, Charge transport anisotropy in hot extruded bismuth telluride: Scattering by acoustic phonons, *J. Appl. Phys.* **128**, 115106 (2020).
- [13] T. Parashchuk, A. Shabaldin, O. Cherniushok, P. Konstantinov, I. Horichok, A. Burkov, and Z. Dashevsky, Enhanced thermoelectric properties of *p*-type Ge_{1-x}Pb_xTe alloys due to decrease of lattice thermal conductivity, *Phys. B (Amsterdam, Neth.)* **596**, 412397 (2020).
- [14] B. Srinivasan, S. L. Tonquesse, A. Gellé, C. Bourgès, L. Monier, I. Ohkubo, J.-F. Halet, D. Berthebaud, and T. Mori, Screening of transition (Y, Zr, Hf, V, Nb, Mo, and Ru) and rare-earth (La and Pr) elements as potential effective dopants for thermoelectric GeTe—an experimental and theoretical appraisal, *J. Mater. Chem. A* **8**, 19805 (2020).
- [15] B. J. H. Lee, J. Wu, and J. C. Grossman, Enhancing the Thermoelectric Power Factor with Highly Mismatched Isoelectronic Doping, *Phys. Rev. Lett.* **104**, 016602 (2010).
- [16] A. Isaeva, B. Rasche, and M. Ruck, Bismuth-based candidates for topological insulators: Chemistry beyond Bi₂Te₃, *Phys. Status Solidi RRL* **7**, 39 (2013).
- [17] O. Caha, A. Dubroka, J. Humlíček, V. Holy, H. Steiner, J. Sanchez-Barriga Ul-Hassan, O. Rader, T. N. Stanislavchuk, A. A. Sirenko, G. Bauer, and G. Springholz, Growth, structure, and electronic properties of epitaxial bismuth telluride topological insulator films on BaF₂ (111) substrates, *Cryst. Growth Des.* **13**, 3365 (2013).
- [18] Y. Xu, Z. Gan, and S.-C. Zhang, Enhanced Thermoelectric Performance and Anomalous Seebeck Effects in Topological Insulators, *Phys. Rev. Lett.* **112**, 226801 (2014).
- [19] E. P. Skipetrov, O. V. Kruleveckaya, L. A. Skipetrova, E. I. Slynko, and V. E. Slynko, Fermi level pinning in Fe-doped PbTe under pressure, *Appl. Phys. Lett.* **105**, 022101 (2014).
- [20] K. Wang, Y. Liu, W. Wang, N. Meyer, L. H. Bao, L. He, M. R. Lang, Z. G. Chen, X. Y. Che, K. Post, J. Zou, D. N. Basov, K. L. Wang, and F. Xiu, High-quality Bi₂Te₃ thin films grown on mica substrates for potential optoelectronic applications, *Appl. Phys. Lett.* **103**, 031605 (2013).
- [21] H. Zhang, C.-X. Liu, X.-L. Qi, X. Dai, Z. Fang, and S.-C. Zhang, Topological insulators in Bi₂Se₃, Bi₂Te₃ and Sb₂Te₃ with a single Dirac cone on the surface, *Nat. Phys.* **5**, 438 (2009).
- [22] I. A. Nechaev and E. V. Chulkov, Quasiparticle band gap in the topological insulator Bi₂Te₃, *Phys. Rev. B* **88**, 165135 (2013).
- [23] S. V. Eremeev, Yu. M. Koroteev, and E. V. Chulkov, Effect of the atomic composition of the surface on the electron surface states in topological insulators A₂^VB₃^{VI}, *Pis'ma Zh. Eksp. Teor. Fiz.* **91**, 419 (2010) [*JETP Lett.* **91**, 387 (2010)].
- [24] O. V. Zazyev, J. E. Moore, and S. G. Louie, Spin Polarization and Transport of Surface States in the Topological Insulators Bi₂Se₃ and Bi₂Te₃ from First Principles, *Phys. Rev. Lett.* **105**, 266806 (2010).
- [25] M. Michiardi, I. Aguilera, M. Bianchi, V. Eustáquio de Carvalho, L. O. Ladeira, N. G. Teixeira, E. A. Soares, C. Friedrich, S. Blügel, and P. Hofmann, Bulk band structure of Bi₂Te₃, *Phys. Rev. B* **90**, 075105 (2014).
- [26] N. P. Stepanov, A. A. Kalashnikov, and O. N. Urupin, Band structure and processes in the electronic system of crystals (Bi_{2-x}Sb_x)Te₃, *Fizika i Technika Poluprovodnikov* **55**, 586 (2021) (in Russian).
- [27] S. A. Nemov, Yu. V. Ulashkevich, A. A. Rulimova, A. E. Demchenko, A. A. Allahkhah, I. V. Sveshnikov, and M. Dzhafarov, On the band structure of Bi₂Te₃, *Semicond.* **53**, 603 (2019).
- [28] I. T. Witting, F. Ricci, T. C. Chasapis, G. Hautier, and G. J. Snyder, The thermoelectric properties of *n*-type bismuth telluride: Bismuth selenide alloys Bi₂Te_{3-x}Se_x, *Research* **2020**, 4361703 (2020).
- [29] B. M. Goltsman, V. A. Kudinov, and I. A. Smirnov, *Thermoelectric Semiconductors Materials Based on Bi₂Te₃* (Nauka, Moscow, 1972) (in Russian).
- [30] B. M. Goltsman, Z. Dashevsky, V. Kaydanov, and N. Kolomoets, *Thin Films: Physics and Application* (Nauka, Moscow, 1986) (in Russian).

- [31] T. Parashchuk, O. Kostyuk, Z. Dashevsky, and L. Nykyruy, High thermoelectric performance of *p*-type $\text{Bi}_{0.5}\text{Sb}_{1.5}\text{Te}_3$ films on flexible substrate, *J. Mater. Chem. Phys.* **253**, 123427 (2020).
- [32] B. Dzundza, L. Nykyruy, T. Parashchuk, E. Ivakin, Y. Yavorsky, L. Chernyak, and Z. Dashevsky, Transport and thermoelectric performance of *n*-type PbTe films, *Phys. B (Amsterdam, Neth.)* **588**, 412178 (2020).
- [33] T. Parashchuk, L. Chernyak, S. Némov, and Z. Dashevsky, Influence of deformation on $\text{Pb}_{1-x}\text{In}_x\text{Te}_{1-y}\text{I}_y$ and $\text{Pb}_{1-x-y}\text{Sn}_x\text{In}_y\text{Te}$ films, *Phys. Status Solidi B* **257**, 2000304 (2020).
- [34] J. Ortega-Castro, N. Hernández-Haro, V. Timón, C. I. Sainz-Díaz, and A. Hernández-Laguna, High-pressure behavior of $2M_1$ muscovite, *Am. Mineral.* **95**, 249 (2010).